Electronic Supplementary Information

for

Microspectroscopic Insight into the Resistivity Switching of Individual Ag-TCNQ Nanocrystals

Benedikt Rösner,[a] Ke Ran,[b] Benjamin Butz,[b] Ute Schmidt,[c] Erdmann Spiecker,[b] and Rainer H. Fink*[a]

[a] *Department Chemie und Pharmazie & ICMM, Friedrich-Alexander-Universität Erlangen-Nürnberg, Egerlandstr. 3, 91058 Erlangen, Germany; E-mail: fink@chemie.uni-erlangen.de*

[b] *Institute of Micro- and Nanostructure Research & Center for Nanoanalysis and Electron Microscopy (CENEM), Friedrich-Alexander-Universität Erlangen-Nürnberg (FAU), Cauerstr. 6, 91058 Erlangen, Germany*

[c] *WITec GmbH, Lise-Meitner-Str. 6, 89081 Ulm, Germany*

Materials and Methods

In situ Raman and STXM experiments

Silver (99.999%) was thermally evaporated onto clean silicon wafers (100 nm SiO_2, purchased from SiMat) in a home-built evaporation chamber under the following conditions: $p \leq 1 \cdot 10^{-7}$ mbar, evaporation rate 0.1-0.3 Å/s, nominal film thickness 30.0 nm as monitored with a quartz crystal balance. A saturated solution of TCNQ (Sigma-Aldrich) in acetonitrile (p.a.) was prepared by stirring an excess of TCNQ in acetonitrile at 50°C for 30 min ($c \approx 5 \cdot 10^{-2}$ M). The reaction was performed by a modified wet-chemical method described in previous studies.[1, 2] The reaction geometry is thereby optimized for obtaining preferably Ag-TCNQ crystallites that are lying individually on the insulating substrate (Fig. S1). Clean silicon wafers with a 100 nm thick oxide layer or silicon nitride membranes are used as substrates. A droplet of 10 µl saturated solution of TCNQ in acetonitrile is then dropped onto the substrates. Subsequently, a 30 nm thick silver layer on silicon is placed upside down on the droplet with a slightly inclined angle (approx. 5-15°). Thereby, Ag-TCNQ crystallites are formed in solution[2] and precipitate on the substrate whereas dendrites – which usually grow on the surface in coexistence to needle-shaped crystallites[3] – are solely formed on the top silver layer. After drying of the solvent, a suiting Ag-TCNQ crystallite ($d = 400 \pm 100$ nm) for in situ STXM and Raman experiments was chosen under the optical microscope and contacted by evaporating gold contact onto the ends of the crystal through a shadow mask (Fig. S2, $p_0 \leq 1 \cdot 10^{-7}$ mbar, evaporation rate 0.1-0.3 Å/s, nominal thickness 30.0 nm). The distance between the gold contacts is 20 µm.

Raman imaging was performed using a WITec alpha 500 R confocal Raman microscope. For *in operando* experiments, the piezo scanner was removed and additional platforms were installed on each side of the motorized scan stage. Two micromanipulators were used to contact the gold pads. The current flow through the contacted Ag-TCNQ crystal was recorded by a Keithley 4200-SCS parameter analyser in sampling mode, *i.e.,* at constant negative voltage over time. Raman spectra of the contacted Ag-TCNQ wire were acquired in spectral imaging mode while the motorized sample stage including

the micromanipulators was scanned in two dimensions. The laser power (232 µW) and dwell time (0.1 ms) were optimized to minimize potential damage to the specimen.

The samples for STXM analysis were prepared similarly on soft X-ray transparent Si_3N_4 membranes (thickness 100 nm, supplier: Silson Ltd., UK). STXM was performed at the PolLux beamline at the Swiss Light Source.[4] A 35 nm Fresnel zone plate was used in combination with an order-sorting aperture to focus the incident X-ray beam onto the specimen. The transmitted intensity was detected by a photomultiplier during 2D scans. The gold contacts were connected to a Keithley sourcemeter outside the measurement chamber, and NEXAFS spectroscopy (0.1 eV spectral resolution) as well as imaging was performed *in operando* with constant negative voltages applied for each data set. Improving the signal-to-noise ratio and thus the data quality by investigating thicker wires is, however, limited by saturation of X-ray absorption at the prominent resonances.

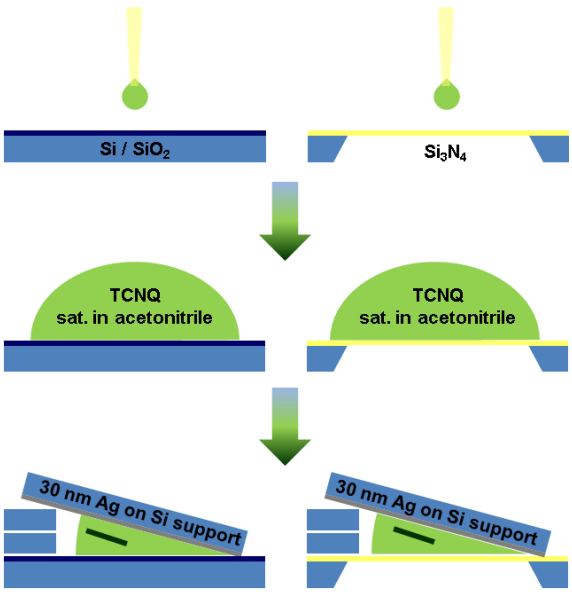

Fig. S1 Wet-chemical synthesis of Ag-TCNQ. The reaction geometry is optimized to obtain preferably individually lying Ag-TCNQ crystallites. Left: sample preparation on a silicon wafer with 100 nm silicon oxide as top layer; right: similar sample preparation on a 100 nm thick Si_3N_4 membrane for X-ray absorption spectroscopy. Two pieces of silicon wafers are used as spacers.

In-situ TEM experiments

Silver (99.999%) was thermally evaporated onto gold TEM grids (G200P purchased from Electron Microscopy Sciences), which were cut into halves using the conditions described above. TCNQ powder (Sigma-Aldrich) and the silver-coated half TEM grids were placed in a flask which was evacuated (< 10^{-2} mbar) and held at 150°C for 2 hours. The specimen was then mounted on a dedicated STM-TEM holder (Nanofactory Instruments) with conductive silver paint. The immovable part of the holder was equipped with a tungsten STM tip (TT10 from Bruker). Moving the specimen by means of a Piezo motor allowed to contacting individual Ag-TCNQ crystallites inside the transmission electron microscope (FEI Titan^3 80-300, acceleration voltage 200 kV). Both the Au TEM grid and the tungsten tip served as the two electrodes for the electrical characterization (the sample was always put on ground). A Keithley 2400 sourcemeter was used for electrical characterization.

Crystallinity

Electron diffraction patterns were acquired to check the crystallinity of the Ag-TCNQ crystallites prepared by wet-chemical synthesis. We observe crystalline Ag-TCNQ (Fig. S2). The wet-chemically prepared Ag-TCNQ was brought into the TEM on lacey carbon TEM grids which were placed on the silicon substrates during preparation (see above).

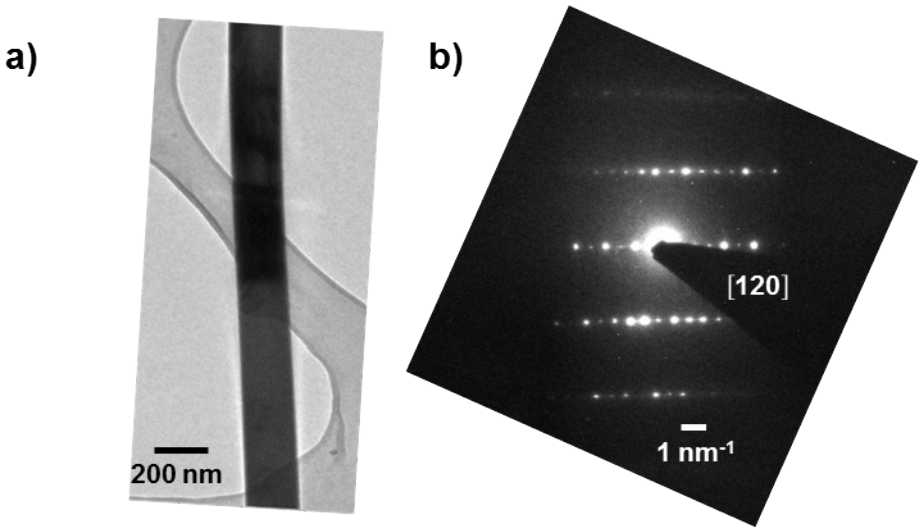

Fig. S2 Crystal structure of Ag-TCNQ: a) bright field image of a wet-chemically prepared nanocrystal and b) its diffraction pattern, showing that the material is single-crystalline.

Data Evaluation and Quantification

Background-correction was performed using a second-order background subtraction for Raman spectroscopy, and by normalizing the pre-edge region to zero and the edge-jump to unity in NEXAFS spectroscopy. The $TCNQ^0$ fraction was determined according to standard procedure for quantification of two species with the corresponding reference spectra. NEXAFS spectra of oriented pristine TCNQ and Ag-TCNQ were taken as references. Each spectrum $\boldsymbol{S}$ was then expressed as a linear combination of spectra $\boldsymbol{S}_{(\mathbf{TCNQ})}$ and $\boldsymbol{S}_{(\mathbf{Ag\text{-}TCNQ})}$:

$$\boldsymbol{S} = \boldsymbol{a} \cdot \boldsymbol{S}_{(\mathbf{TCNQ})} + (1-\boldsymbol{a}) \cdot \boldsymbol{S}_{(\mathbf{Ag\text{-}TCNQ})} + \boldsymbol{C} \quad (1)$$

($\boldsymbol{C}$ is a constant which is negligible small).

Reference Spectra

Raman and NEXAFS spectroscopy allow to differentiating between neutral TCNQ molecules and TCNQ anions by their typical vibrational fingerprint and unoccupied molecular orbitals. Whereas most of the vibration bands retain approximately the same Raman shift, the vibrational band at 1457 rel. cm^{-1} of the neutral TCNQ molecule is red-shifted by 69 wavenumbers in Ag-TCNQ by the uptake of one electron (Fig. S3).

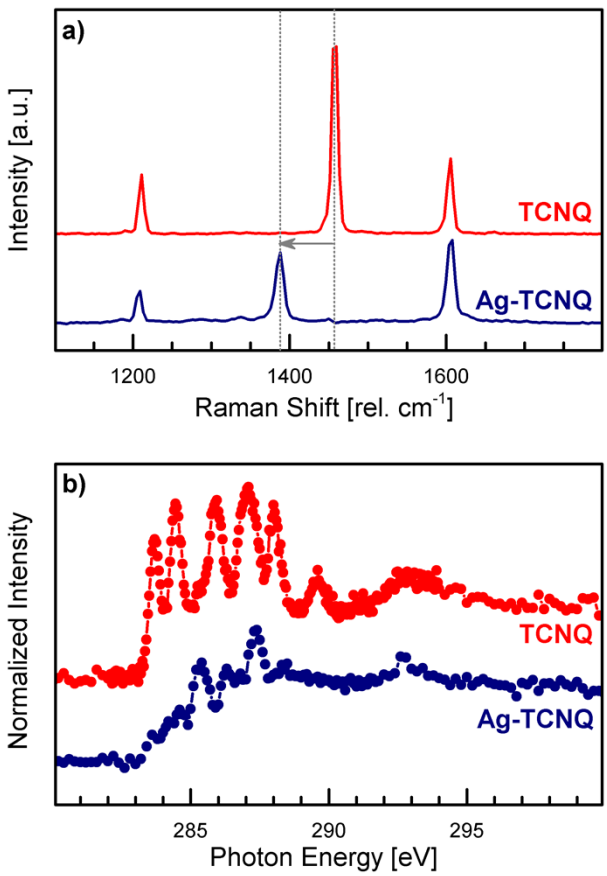

Fig. S3 Reference spectra of TCNQ (red) and Ag-TCNQ (blue). a) Raman spectra, and b) NEXAFS spectra. Note that the E-vector is oriented out of the molecular TCNQ plane to maximize the C 1s → π* transitions of the ring system.

Decomposition of Ag-TCNQ by Heating

At currents which exceed 10^{-7} to 10^{-6} A, the Ag-TCNQ wires start to decompose. The failure is accompanied by substantial thinning of the crystallites until they are completely ripped. The explanation for this effect is current-induced heating whereas decomposition occurs in the middle between STM tip and TEM grid where the most heat is accumulated and thermal dissipation is most unlikely. Neutral TCNQ is formed and can sublime into the vacuum and neutral silver remains on the crystal and forms the black particles visible in Fig. S4.

When heating Ag-TCNQ locally using excessively high laser intensities, decomposition of the crystallites is also observed, accompanied by condensation of neutral TCNQ around the irradiated parts of the crystal (Fig. S5). Apparently, the irradiation time plays a critical role as decomposition seems to start when the thermal energy introduced by intense irradiation dissipates slower than the laser heats up the specimen. This becomes obvious from the fact that the part of the crystal which is oriented parallel to the main scan direction is decomposed whereas the other crystallite with a slightly inclined angle with respect to the line scan direction is not damaged (Fig. S5b-e). We therefore optimized the laser intensity before performing the switching experiments and set the scan direction accordingly to scan lines perpendicularly across the Ag-TCNQ wires. Note that the crystal presented here is by an order of magnitude larger in diameter than the crystallites investigated *in operando* for better visibility in the optical microscope of the confocal Raman microscope.

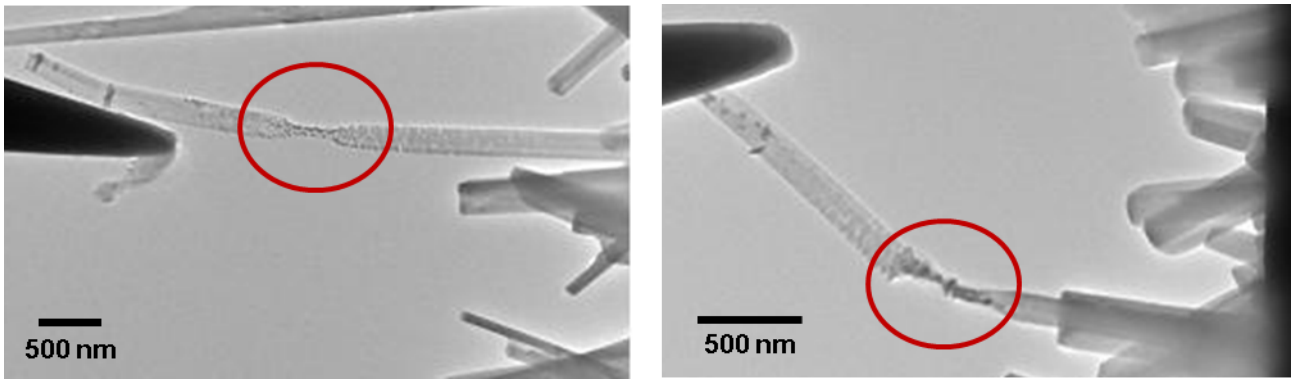

Fig. S4 Thinning and rupture of Ag-TCNQ wires upon too high current flow in the TEM. The crystallites become thinner in the middle where the most heat is accumulated as it can only dissipate towards the sample support or the tip in ultrahigh vacuum.

5

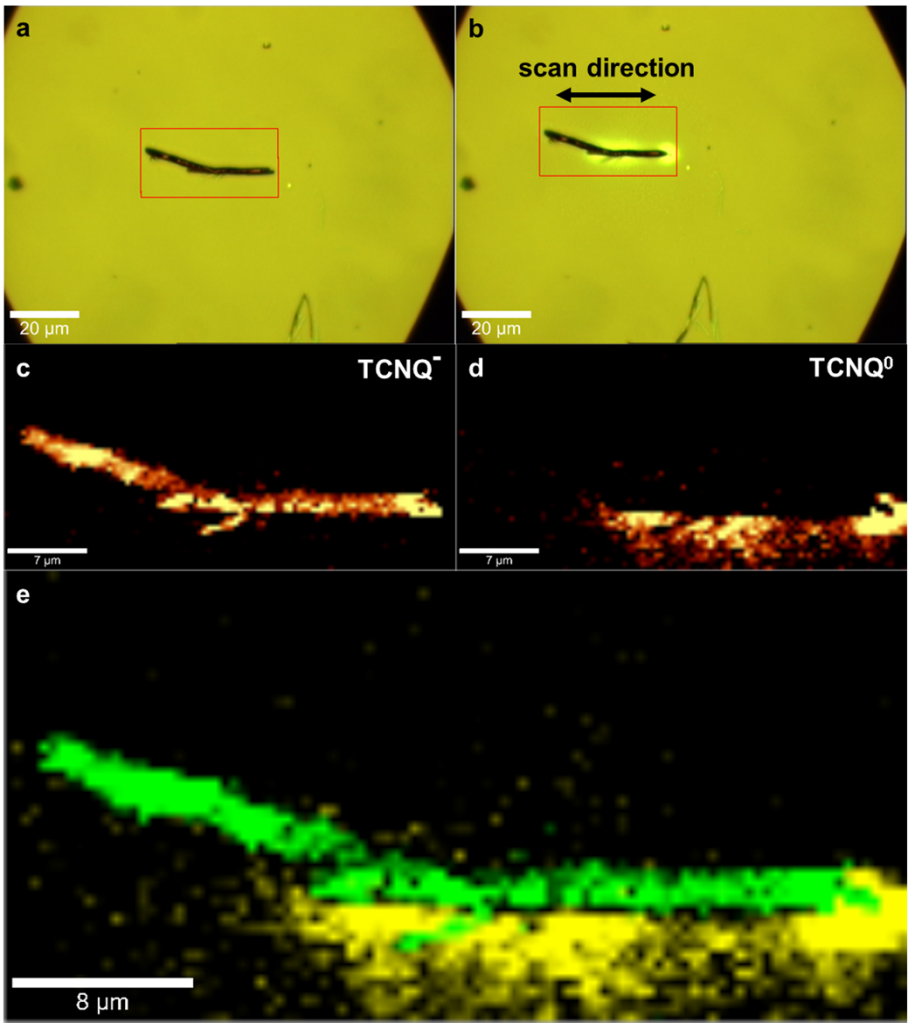

Fig. S5 Evaporation of TCNQ at intense laser power. a) Optical micrograph before and b) after scanning with too high laser intensity. The line scan direction is from left to right. c) Bandpass filter showing the peak intensity at 1388 rel. cm^{-1}, corresponding to Ag-TCNQ. d) Bandpass filter showing the peak intensity at 1457 rel. cm^{-1}, corresponding to TCNQ. e) Overlay of c) and d), visualizing the evaporation of TCNQ around the crystallite.

1. G.-Y. Cao, C.-N. Ye, F. Fang, X.-Y. Xing, H.-H. Xu, D.-L. Sun and G.-R. Chen, *Materials Science and Engineering B*, 2005, **119**, 41-45.
2. B. Rösner, A. Späth and R. H. Fink, *J. Cryst. Growth*, 2013, **380**, 34-38.
3. G.-Y. Cao, F. Fang, C.-N. Ye, X.-Y. Xing, H.-H. Xu, D.-L. Sun and G.-R. Chen, *Micron*, 2005, **36**, 285-290.
4. J. Raabe, G. Tzetkov, U. Flechsig, M. Böge, A. Jaggi, B. Sarafimov, M. G. C. Vernooij, T. Huthwelker, H. Ade, D. Kilcoyne, T. Tyliszczak, R. H. Fink and C. Quitmann, *Rev. Sci. Instrum.* , 2008, **79**, 113704.